Solid-State Approach for Fabrication of Photostable, Oxygen-Doped Carbon Nanotubes

Xuedan Ma, Jon K. S. Baldwin, Nicolai F. Hartmann, Stephen K. Doorn, and Han Htoon**

A novel procedure for effective fabrication of photostable oxygen-doped single-walled carbon nanotubes (SWCNTs) in solid-state matrices has been developed. SWCNTs drop-cast on various types of substrates are coated with oxide dielectric thin films by electron-beam evaporation. Single tube photoluminescence spectroscopy studies performed at room and cryogenic temperatures reveal that such thin film-coated tubes exhibit characteristic spectral features of oxygen-doped SWCNTs, indicating the oxide thin film coating process leads to oxygen doping of the tubes. It is also found that the doping efficiency can be effectively controlled by the thin film deposition time and by the types of surfactants wrapping the SWCNTs. Moreover, aside from being the doping agent, the oxide thin film also serves as a passivation layer protecting the SWCNTs from the external environment. Comparing the thin film coated SWCNTs with oxygen-doped tubes prepared via ozonolysis, the former exhibit significantly higher photostability and photoluminescence on-time. Therefore, this one-step deposition/oxygen-doping procedure provides a possible route toward scalable, versatile incorporation of highly photostable oxygen-doped SWCNTs in novel optical and optoelectronic devices.

1. Introduction

Semiconducting single-walled carbon nanotubes (SWCNTs) are promising candidate materials for a wide range of photonic applications due to their unique electronic and optical properties.[1–6] Moreover, the recent discovery that covalent sidewall doping of SWCNTs can lead to a strong red-shift of emission and more than an order of magnitude enhancement of emission efficiency[7–9] not only makes these applications more feasible but also enables new functionalities that were not accessible before. Particularly, by localizing one dimensional excitons of SWCNTs into optically active deep traps located more than 130 meV below the band gaps,[10] the dopant states of SWCNTs may open new routes toward realizing population inversion needed for lasing[11] and have recently been shown to provide a route to room temperature single photon generation at telecommunication wavelength for quantum communication applications.[12]

Realization of this potential, however, is currently hindered by a few critical material issues. Firstly, while current methods of controlled doping are low cost and can produce large amounts of doped SWCNTs, they typically involve prolonged exposure (from hours to days) of SWCNTs to doping agents in aqueous suspensions under careful monitoring of the doping agent dose and surfactant concentration.[7,9] A solid state approach enabling controlled doping of SWCNTs fabricated via chemical vapor deposition and of SWCNTs that have already been integrated into devices is highly desirable. Secondly, while the resultant doped tubes exhibit reasonable photoluminescence (PL) stability in their native solution environment,[9] their PL emission shows rapid fluctuations both in intensity and energy when placed on solid state substrates.[10] These fluctuations must first be eliminated for any optoelectronic applications. Thirdly, because unprotected SWCNTs can readily be damaged, a solid-state matrix capable of maintaining, and stabilizing the optical properties of doped SWCNTs is also needed. Finally, for further device integration, such a matrix is also required to be compatible with existing microelectronic fabrication technologies.

Here, we present a novel solid state doping approach capable of resolving these outstanding challenges. Our approach is substantially different from, and more amenable to enable optoelectronic applications than available doping methods in aqueous suspensions. In our case, undoped SWCNTs deposited on substrates are directly coated with a thin SiO_2 film by electron beam evaporation. Coating of the oxide dielectric films on one hand leads to rapid oxygen-doping of the SWCNTs, and on the other hand protects them from external environmental fluctuations, resulting in significant photostability. By monitoring the oxygen partial pressure during deposition, we identify dissociation of the oxides during evaporation as the mechanism responsible for the doping. We also demonstrate that oxide film thickness and types of surfactants can be utilized to control the efficiency of doping and this solid state doping approach can also be extend to other technologically important dielectric

Dr. X. Ma,[+] J. K. S. Baldwin, Dr. N. F. Hartmann, Dr. S. K. Doorn, Dr. H. Htoon
Center for Integrated Nanotechnologies
Materials Physics and Applications Division
Los Alamos National Laboratory
Los Alamos, NM 87545, USA
E-mail: skdoorn@lanl.gov; htoon@lanl.gov

[+]Present address: Center for Integrated Nanotechnologies, Sandia National Laboratories, Albuquerque, NM 87185, USA

DOI: 10.1002/adfm.201502580

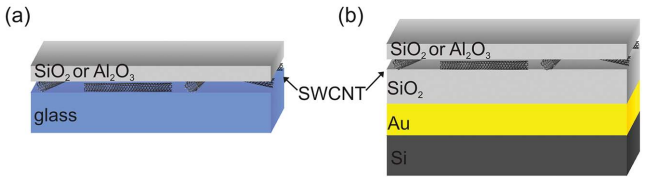

Figure 1. a,b) Cross-sectional schematics of the oxide dielectric thin film coated SWCNT matrices. Different substrates and oxide source materials can be flexibly employed in the fabrication process.

oxide films such as Al_2O_3. By providing dopant states with ultrastable PL emission, this novel approach recently enabled us to demonstrate room temperature single photon generation from solitary oxygen dopant states of SWCNTs.[12] Furthermore, because our new approach allows fabrication of the SiO_2 encapsulated SWCNTs on top of a silicon wafer, the doped SWCNTs are readily compatible with well-established microelectronic fabrication technology. Their integration into electronic and photonic circuits thus becomes more feasible. This approach will therefore further enable development of doped SWCNT based electrically driven quantum/classical light sources[13–15] and other quantum controlled devices.[16] Beyond this, our approach should be extendable to create thin films of doped SWCNTs for lasing and other opto-electronic applications.

2. Results and Discussion

Figure 1a,b shows cross-sectional schematics of the oxygen-doped SWCNT matrices fabricated in this study. Typically, samples enriched in undoped (6,5) SWCNTs are drop-cast on substrates (such as glass cover slides or quartz substrates, Figure 1a). Then a thin layer of SiO_2 or Al_2O_3 dielectric film is directly deposited on top by electron beam evaporation (see the Experimental Section for details). In order to perform optical measurements on substrates that give background emission in the near-infrared range such as Si (Figure 1b), a layer of Au film is deposited first to shield the Si background emission, and then a thin layer of SiO_2 is deposited to prevent PL quenching of the tubes due to direct contact with the Au film.

To investigate the effects of oxide thin film coating on the electronic structures of the SWCNTs, we studied the optical properties of individual SWCNTs both at room and cryogenic temperatures. Undoped SWCNTs without the thin film coating were studied as references. **Figure 2**a presents a typical room

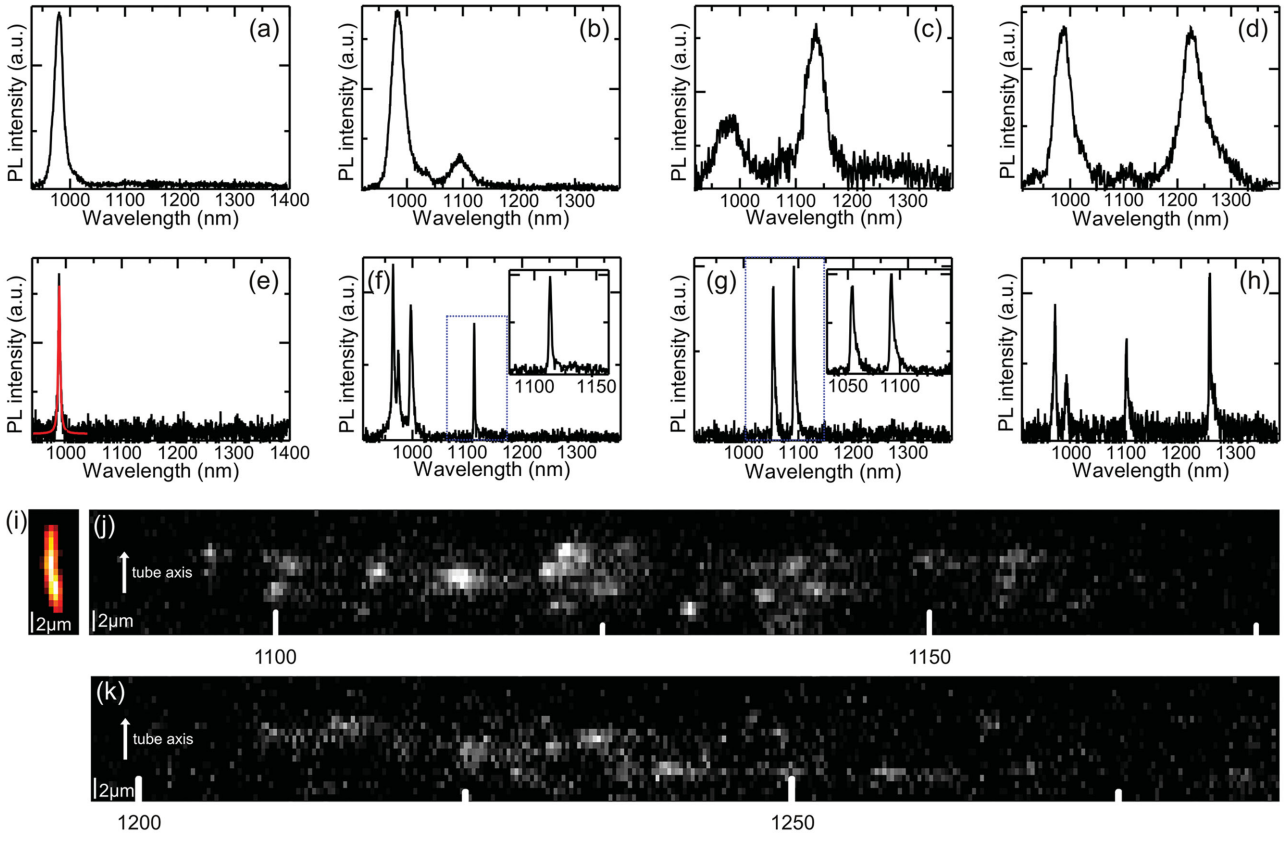

Figure 2. Optical spectra of a,e) individual undoped) and b–d, f–h) SiO_2 thin film coated SWCNTs at a–d) room and e–h) cryogenic temperatures. The red curve in (e) is a Lorentzian fit to the PL peak. Insets in (f) and (g) are the enlarged views of the blue marked areas. It can be clearly observed that the dopant-induced peaks are asymmetric with long tails at the low energy side. i) A wide field PL image of an individual SiO_2 thin film coated SWCNT at 4.2 K taken for all PL emission wavelengths longer than 930 nm. Uniform PL emission along the tube axis can be observed. j,k) Spatially resolved PL spectra of the tube in (i). Vertical positions in (j) and (k) correspond directly to that in (i). Discrete, asymmetric peaks centering at ≈1120 and 1240 nm can be observed at different positions along the tube.

temperature PL spectrum for an individual undoped tube, where a single peak at ≈980.1 nm can be observed. Of the 33 undoped tubes studied at room temperature, 31 of them exhibit single peaks in the wavelength range of 971–1035 nm, which corresponds to the well-known bright E_{11} exciton emission (see Figure 5a for statistics and ensemble PL spectrum). In contrast, for tubes coated with SiO_2 thin films, additional peaks mainly centered at ≈1100 (E_{11}^{*}) and ≈1250 nm (E_{11}^{*-}) can be observed, as shown in Figure 2b–d. The percentage of tubes showing these additional peaks strongly depends on such experimental conditions as film deposition time and choice of surfactants used to generate the initial aqueous SWCNT suspensions (see below for detailed discussion).

We further studied individual SWCNTs at cryogenic temperatures. Figure 2e shows a representative PL spectrum (black curve) of an individual undoped SWCNT at 4.2 K fitted with a Lorentzian function (red curve). The peak is centered at 988.3 nm with a full width at half maximum of 3.9 nm, close to previously reported low temperature single tube spectral line width values.[1,6,10,17,18] Different from the undoped tubes, SWCNTs embedded in SiO_2 thin films typically exhibit two characteristic spectral features at cryogenic temperatures: (1) Splitting of the E_{11} peak at ≈980 nm into two–three symmetric peaks with splitting energy smaller than 40 meV (Figure 2f,h); (2) Emergence of additional peaks at ≈1100 and ≈1250 nm that are highly asymmetric, with long tails at the low energy side (Figure 2f–h and insets). These spectroscopic features at cryogenic temperatures are characteristic of previously reported oxygen-doped SWCNTs prepared via ozonolysis:[10] While the splitting of the E_{11} peak is attributed to brightening of dark states through defect-induced symmetry breaking, the new asymmetric peaks at ≈1100 (E_{11}^{*}) and ≈1250 nm (E_{11}^{*-}) are due to doping-introduced deep trap states associated with different chemical adducts (specifically, the peak at ≈1100 nm is associated with ether groups, and the one at ≈1250 nm to epoxides).[10] Typically, the asymmetric line and shape of these features is attributed to interactions between localized excitons and 1D phonons.[1,17] Based on these spectroscopic features, it is reasonable to conclude that oxide dielectric thin film coating of SWCNTs leads to covalent oxygen doping of the tubes. This covalent oxygen doping is in stark contrast to charge-transfer doping that can occur with adsorbed oxygen species,[19–21] which is known to bleach ground state absorption and quench normal E_{11} exciton emission in SWCNTs; quite the opposite of the enhanced emission behavior observed from the covalent dopant sites. This result thus highlights a broader view of dopants as added impurities or defects that introduce new electronic states with added functionality beyond acting to simply inject new charge carriers. This is an important perspective for enhancing a wide range of nanomaterial functionality.[22]

Observation of multiple new peaks at ≈1100 and ≈1250 nm (Figure 2g,h) further confirms that multiple trap sites with the same (e.g., Figure 2g, both are ether groups) and/or different (e.g., Figure 2h, ether and epoxide groups) chemical adducts can coexist on a single tube. While dopant emission in most cases originates from diffraction limited spots, indicating that doping usually occurs in isolated locations, in some cases, we observe spreading of the dopants along the length of the tube. Figure 2i shows a wide field PL image of an individual SiO_2-coated SWCNT, where uniform PL emission along the tube can be observed. However, spatially resolved optical spectra of the tube along its axis show many distinct asymmetric PL peaks at different wavelengths, mainly centering at ≈1120 and 1240 nm. These position-dependent PL spectra provide further evidence that the SiO_2 coating process can create multiple localized trap states of different chemical natures along the tube. While different chemical adducts can coexist on a single tube (Figure 2h), variation of the local dielectric environment can lead to different transition energies for the same type of chemical adducts (Figure 2g).[10]

Towards understanding the doping mechanism during the SiO_2 dielectric thin film deposition procedure, we first note that the extremely low concentration of residual O_2 from air in the deposition chamber (mean O_2 partial pressure = 1.38×10^{-11} Torr) and its relatively low reactivity make the residual O_2 in the chamber an unlikely doping agent. To support this, we found that exposure to air of surfactant wrapped SWCNTs deposited on glass cover slides for several weeks shows no sign of oxygen doping. Furthermore, undoped SWCNTs incorporated in MgF_2 thin films by electron beam evaporation remained mostly undoped. Therefore, our first assumption is that during the electron beam evaporation procedure, reactive species that are capable of acting as dopants are generated. This is based on the common finding in thin film studies that most inorganic compounds evaporate with molecular changes, and the vapor composition is usually different from that of the original source.[23,24] For oxides, evaporation is often accompanied by dissociation, and high oxides dissociate to lower oxides:[23,24] MO_2 (s) → MO (g) + (1/2) O_2 (g), where M = metal. To test the hypothesis that it is mainly the dissociation of oxides that causes the oxygen doping effect, we employed another oxide, Al_2O_3, instead of SiO_2 as an alternative coating source material. We found that similar oxygen-doping effects were observed (see Section S1, Supporting Information for details). We also monitored the change in O_2 partial pressure during a 5 nm SiO_2 thin film electron beam evaporation procedure, as shown in **Figure 3**a. Before heating and deposition, the O_2 partial pressure in the chamber was close to zero. When heating by electron beam starts, the partial pressure gradually increased and finally stabilized at $\approx 7.49 \times 10^{-10}$ Torr during SiO_2 film deposition. Once heating is stopped, the O_2 partial pressure decreased back to zero. The results shown in Figure 3a clearly indicate that oxidizing agents (mainly SiO and O_2 in this case) were generated during the SiO_2 evaporation and dissociation processes. These species are likely highly reactive as a result of their absorption of energy from the electron beam, thus serving as the oxygen doping agents to the SWCNTs, as shown schematically in Figure 3b. Therefore, we conclude that oxygen doping during the electron beam evaporation coating process is mainly, if not completely, due to dissociation of the oxide source materials (e.g., SiO_2 and Al_2O_3).

Having established the origin of oxygen-doping in the oxide thin film coated SWCNTs, we study the influence of different factors affecting the doping process. We first study the influence of thin film deposition time, which is directly quantified by the film thickness at a constant deposition rate. Sodium dodecylbenzene sulfonate (SDBS) wrapped SWCNTs were coated with different thicknesses of SiO_2 films (0.5–280 nm),

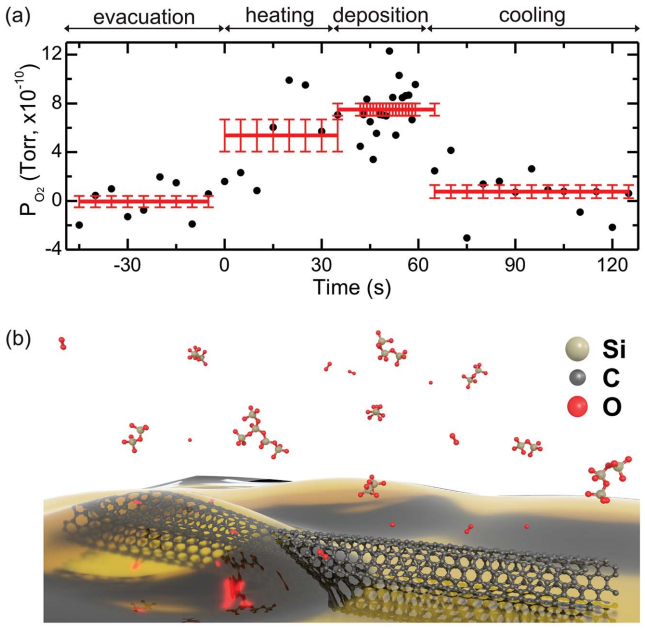

Figure 3. a) O_2 partial pressure (Po_2) in the deposition chamber at the different stages of the electron beam evaporation of a 5 nm thick SiO_2 film onto a SWCNT sample at the deposition rate of 0.2 nm s^{-1} (black dots). Time ranges corresponding to the different stages are marked at the top. Average O_2 partial pressures in the deposition chamber for the four different stages are plotted as horizontal red lines together with the corresponding standard errors. b) A schematic of the oxygen-doping mechanism during the oxide thin film evaporation process. Dissociation of SiO_2 due to electron beam bombardment mainly generates vapor phase SiO and O_2 which serve as the doping agents for SWCNTs.

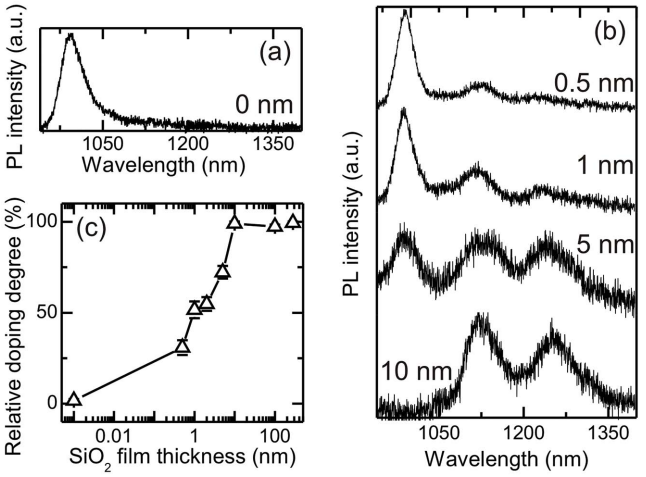

Figure 4. a,b) Room temperature ensemble PL spectra of SDBS wrapped SWCNTs coated with different thicknesses of SiO_2 thin films. SiO_2 film thicknesses are marked at the side of each spectrum. For a) tubes without SiO_2 thin film coating, a single peak at ≈992.9 nm can be observed, while for b) those coated with SiO_2 films, additional peaks at ≈1120 and 1250 nm appear, and their intensities increase with the SiO_2 film thickness (from top to bottom). c) SiO_2 film thickness-dependent relative doping degree, which is defined as the ratio between the PL intensity of the dopant-introduced peaks (>1045 nm) and the overall PL intensity, and averaged over ensemble PL spectra taken at five to ten different positions. The relative doping degree increases with the SiO_2 film thickness, and reaches 100% at the film thickness of 10 nm.

and ensemble PL spectra were taken for each sample at room temperature. As expected, for undoped SWCNTs without SiO_2 coating (**Figure 4**a), a single peak at ≈992.9 nm can be observed. For SiO_2 thin film coated tubes, additional peaks at ≈1120 and 1250 nm, attributed to ether and epoxide adducts, respectively, appear (Figure 4b). With the increase of the coating film thickness, i.e., deposition time, PL intensity of the dopant introduced peaks at 1120 and 1250 nm increases while that of the E_{11} peak at ≈990 nm decreases, indicating an increasing dopant concentration. As shown in Figure 4c, at a SiO_2 film thickness of only 1 nm, the relative doping degree (defined as the ratio between the PL intensity integrated over all the doping introduced peaks (>1045 nm), and the total spectrally integrated PL intensity) averaged from ensemble PL spectra taken at five to ten different positions, has already reached 51.6%, indicating a very efficient doping process. At a SiO_2 film thickness of 10 nm, the relative doping degree has reached 100%, and remains constant to SiO_2 film thickness of up to 280 nm, the thickest film fabricated in this study. The continued doping of SWCNTs at SiO_2 film thicknesses larger than 1 nm (note that the tube diameter is ≈0.8 nm) indicates that either the tubes have not been completely covered at this level of deposition or that the doping species are trapped in the solid-state matrices. Detailed study is needed to further understand the mechanism behind this. At the normal deposition rate of 0.2 nm s^{-1}, it only takes 50 s to deposit a SiO_2 film with a thickness of 10 nm and to reach the complete doping of all tubes. Compared to oxygen-doping in aqueous SWCNT suspensions (typically taking hours to days to reach complete doping of the tubes),[8–10] this solid-state process is significantly more efficient.

We also investigated the influence of the particular surfactants used for SWCNT wrapping on the thin film doping process. Three commonly used surfactants, including sodium deoxycholate (DOC),[25–27] SDBS,[28–30] and sodium dodecylsulfate (SDS)[31–34] wrapped (6,5) SWCNTs were drop-cast on precleaned glass cover slides, and coated with 10 nm SiO_2 thin films. Single tube PL spectra of the three different types of samples were studied at room temperature for a total of 144 tubes. Histograms in **Figure 5**b–d show PL peak distributions of the tubes wrapped with different surfactants. It can be seen that for tubes wrapped with DOC, the doping efficiency is much lower than those of the SDBS and SDS wrapped tubes. Specifically, with the SiO_2 film thickness of 10 nm, only ≈56% of the DOC wrapped tubes (23 out of 41 tubes) show additional dopant introduced peaks, while more than 95% of the SDBS and SDS wrapped tubes (61 out of 62 for SDBS wrapped tubes, and 39 out of 41 for SDS wrapped tubes) became oxygen doped. This trend is consistent with the room temperature ensemble PL spectra shown in Figure 5b–d (black curves). For DOC wrapped SWCNTs the E_{11} peak dominates the PL spectrum. However, it almost disappears for the SDBS and SDS wrapped tubes, and instead, the dopant introduced PL peaks at ≈1120 and 1250 nm dominate.

To show this more clearly, we took wavelength-dependent wide field PL images with specific optical filters of the three different types of samples coated with 10 nm SiO_2 thin films. In Figure 5e–h, the upper panels are PL images of the tubes

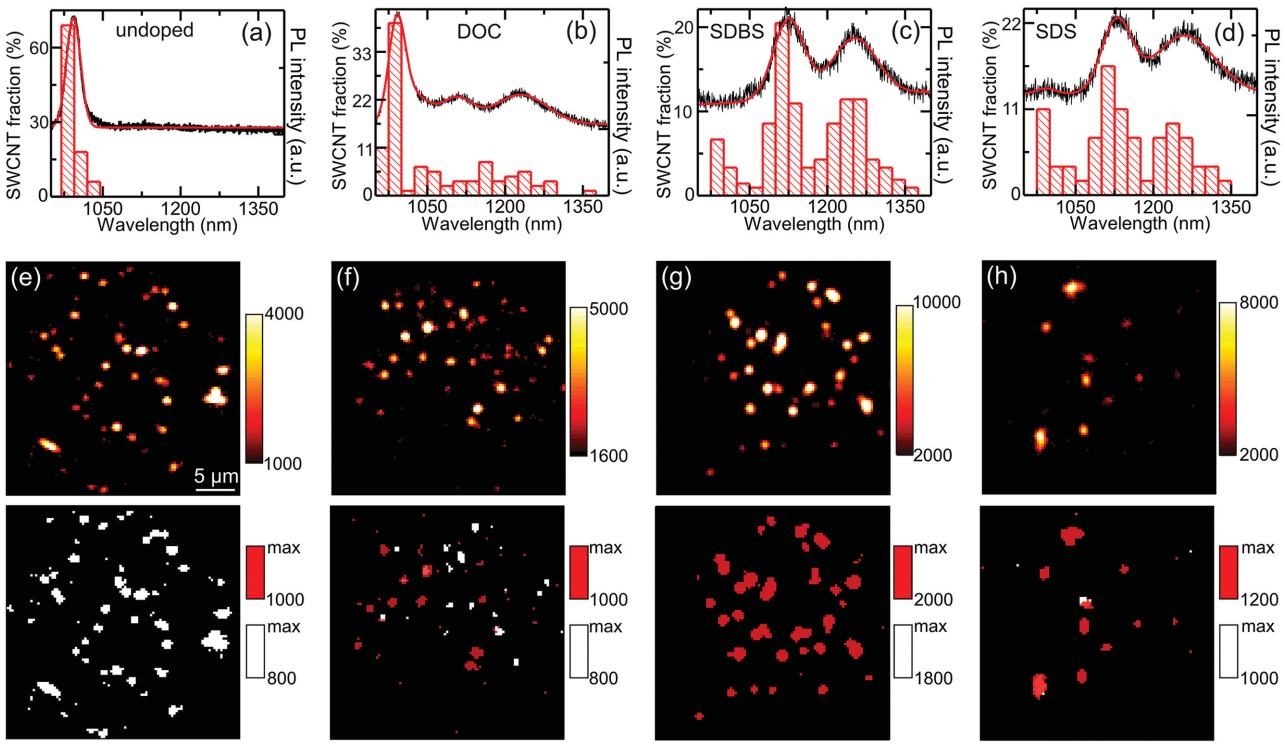

Figure 5. a–d) Histograms: Room temperature single tube PL spectral peak distributions of a) undoped tubes, and b) DOC, c) SDBS, and d) SDS wrapped SWCNTs coated with 10 nm thick SiO_2 films. Black and red curves: Room temperature ensemble PL spectra (black curves) of the different samples fitted with sums of multiple Gaussian functions (red curves). e–h) Upper panels: Wide field PL images of e) undoped tubes, and 10 nm thick SiO_2 film coated f) DOC, g) SDBS, and h) SDS wrapped SWCNTs in the wavelength range of >930 nm (thus including emissions from all the peaks). Lower panels: Wide field PL images of e) undoped tubes, and 10 nm thick SiO_2 film coated f) DOC, g) SDBS, and h) SDS wrapped SWCNTs in the wavelength range of 975–1025 nm (white color, corresponding to E_{11} peak) and >1045 nm (red color, corresponding to doping introduced E_{11}^{*} and E_{11}^{*-} peaks). The PL imaging integration time for the different samples and wavelengths was kept the same, namely, 10 s.

taken for all PL emission wavelengths longer than 930 nm (i.e., capturing emission from all possible origins), and in the lower panels, PL emission with wavelengths in the range of 975–1025 nm (corresponding to the E_{11} peak) and >1045 nm (corresponding to the E_{11}^{*} and E_{11}^{*-} peaks) is presented by white and red colors, respectively. As expected, the undoped tubes (Figure 5e) show only PL emission in the wavelength range of 975–1025 nm (white color). For the thin film coated tubes, the difference between the DOC wrapped tubes and SDBS/SDS wrapped tubes is significant. While many of the DOC wrapped tubes emit in the E_{11} peak regime (Figure 5f, lower panel, white color), emission of the SDBS/SDS wrapped tubes is dominated by PL with wavelength >1045 nm (Figure 5g,h, lower panel, red color), which is consistent with the PL spectral measurements shown in Figure 5b–d. This difference, we believe, is related to the different molecular structures, and consequently the wrapping mechanisms of the three different surfactants. Several studies have shown that DOC provides much better suspension quality compared to other surfactants.[25,27] The reason for this is that bile salts such as DOC tend to form a compact, homogeneous micelle structure around the SWCNTs due to their rigid, steroid-ring structures.[35] Such surface structures tend to inhibit access to the SWCNT surface by reactive dopant species. By contrast, linear, rod-like surfactants such as SDS and SDBS usually favor a sparse, disordered micelle structure[32,34,36,37] that permits easy access of dopants to the SWCNT surface. Although collapse of surrounding surfactant micelles during drying is expected to happen, the difference in the wrapping mechanisms of the surfactants is still sufficient to lead to different surface coatings of the tubes, and consequently the doping efficiencies.

The above two factors, i.e., oxide film deposition time and surfactant wrapping type, provide useful means to effectively control the dopant concentrations of the SWCNT samples. Based on these results, we believe our oxide thin film doping procedure has potential for applications to tubes grown directly on substrates by chemical vapor deposition methods,[38–40] for which the doping efficiency might be even higher compared to those dispersed in suspension by surfactants. This is probably another advantage of this oxide thin film doping method, i.e., it is a general method that may be potentially applied to different types of carbon nanotubes.

In addition to the efficiency and convenience, we also find that the oxide thin film coating of SWCNTs provides a route to more stable PL emission than is found for those doped via ozonolysis in aqueous suspension. To estimate the stability of the tubes, we continuously illuminated them with a quasi-homogeneous, expanded (≈60 × 60 μm) continuous-wave laser beam (840 nm, ≈20 mW) and recorded their time-dependent PL images (see the Supporting Information for videos). Freshly prepared SDBS wrapped tubes doped via ozonolysis were deposited on precleaned glass cover slides for reference. **Figure 6**a,b

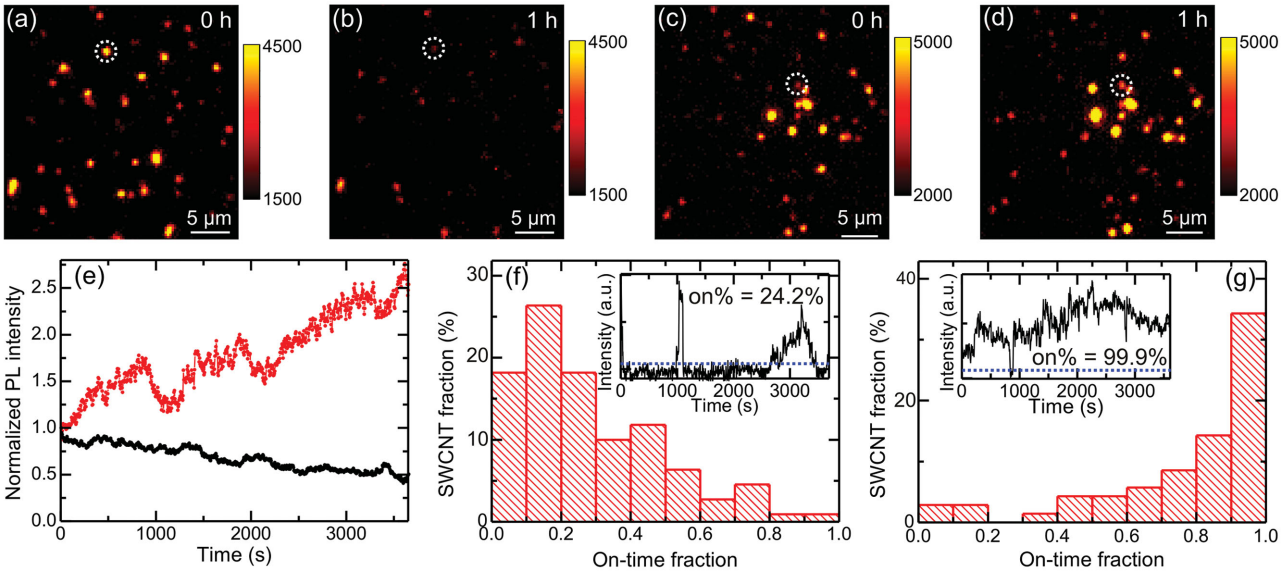

Figure 6. a–d) Wide field PL images (integration time was 5 s) of tubes doped by a,b) ozonolysis and c,d) SiO_2 thin film coating at a,c) the beginning of irradiation and b,d) after continuous laser irradiation for 1 h with a continuous-wave laser (840 nm, ≈20 mW) expanded to a quasi-homogeneous spot (≈60 × 60 μm). e) Time dependent overall PL intensities of all the tubes in (a) (black) and (c) (red) extracted from the wide field PL images. f,g) Distributions of on-time fractions calculated from PL time traces of tubes doped by f) ozonolysis and g) SiO_2 thin film coating. Insets: Representative PL time traces of the tubes circled in (a,b) (corresponding to inset of (f)) and (c,d) (corresponding to inset of (g)) with a time bin of 5 s. The blue dashed lines are the thresholds defined as twice the mean background level. States above the thresholds are on-states, and those below are off-states. On-time fractions of 24.2% and 99.9% are obtained for the time traces in the insets of (f) and (g), respectively.

shows PL images of tubes doped via ozonolysis at the beginning of the irradiation and after being continuously irradiated for 1 h, respectively. Time evolution of the combined PL intensities from all the tubes in the images is shown in Figure 6e. For tubes doped via aqueous-phase ozonolysis (Figure 6e, black curve) significant PL quenching can be observed. After being irradiated for 1 h, the overall PL intensity of these tubes has decreased to only 50% of their original value. A similar quenching was also observed in time-dependent PL spectra of individual doped tubes at low temperatures as shown in Figure S2a,b (Supporting Information). The data further show that the decrease of the dopant emission does not lead to any increase in emission of the E_{11} transition. Bleaching of both transitions is instead observed in some cases (Figure S2b, Supporting Information). We therefore rule out photoinduced reversal of oxide species as a possible mechanism for this bleaching behavior since such a process should lead to partial restoration of E_{11} emission. We postulate photodegradation of surfactant micelles that leads to creation of new exciton quenching sites as a cause of bleaching. The temporal photostability is therefore expected to be higher for tubes with intact surfactant layers in aqueous suspension[21] or embedded in aqueous silica gels.[41] We also extracted PL time traces of the tubes from the time-dependent wide field PL images. PL time traces of ≈110 ozonolysis doped tubes were studied. By choosing a threshold that is twice the mean background level,[42] we are able to define the on- and off-states of the tubes, and calculate the on-time fraction, which is defined as the ratio between the time that a tube is in the on-state and the total irradiation time. Distribution of the on-time fraction of the tubes doped via ozonolysis is shown in Figure 6f, and almost 80% of the studied tubes are in the on-state for less than 50% of the irradiation time. For many tubes, photobleaching can be observed. A representative PL time trace from the tube marked in Figure 6a,b is shown in the inset of Figure 6f. An on-time fraction of only 24.2% is observed in the 1 h irradiation time for this specific tube.

The above results from the control samples are in stark contrast with those obtained for the thin film coated tubes. Figure 6c,d shows wide field PL images of 10 nm SiO_2 thin film coated tubes wrapped with SDBS at the beginning of the experiment and after being continuously irradiated for 1 h, respectively. Not only did most of the tubes continue to emit, but we also observed the emergence of emission from several previously "dark" tubes. The time evolution of the summarized PL intensities from all these tubes in the images (Figure 6e, red curve) indicates significant brightening of dopant emission is happening to the thin film coated tubes during the irradiation. After continuous irradiation for 1 h, the overall PL intensity increases to 2.5 times of the initial value. A similar behavior is also observed in the low T PL spectra of individual thin film coated tubes as shown in Figure S2c,d (Supporting Information). This spectral data further reveal that both E_{11} and E_{11}^{*} transitions were brightened. Such photobrightening has been observed in various types of semiconductor quantum dots (QDs) such as core and core-shell CdSe QDs,[43–45] PbS,[46] ZnSe,[47] doped ZnS,[48] and CuBr[49] QDs. Although the exact mechanism remains controversial, it is commonly accepted that photobrightening can result from passivation of surface trap states, which decreases the possibility of excitons recombining nonradiatively and in turn increases the PL intensity.[45,47] The photobrightening phenomena we observed in thin film coated tubes may be due to a similar mechanism. Further studies, however, are necessary to fully understand this behavior. On-time fractions calculated from time traces of 70 thin film coated

tubes are presented in Figure 6g. Nearly, 50% of the tubes show on-time fractions larger than 80%, indicating very stable PL emission. A representative PL time trace from one of the thin film coated tubes marked in Figure 6c,d is shown in the inset of Figure 6g, where the tube exhibits an on-time fraction of 99.9% in the 1 h irradiation time. These results clearly demonstrate that the photostability afforded by thin film coating of the tubes significantly surpasses that of the tubes doped by ozonolysis in aqueous suspension.

3. Conclusion

In summary, oxide thin film coating of undoped SWCNTs leads to observation of new PL peaks with characteristic spectral features of oxygen-doped tubes. We attribute this kind of oxygen-doping to dissociation of oxides during electron beam evaporation. We also find that the oxygen-doping efficiency during thin film deposition is strongly dependent on the oxide thin film deposition time and the kinds of surfactants wrapping the tubes. Such experimental factors provide useful means to effectively control the dopant concentrations of the tubes. Moreover, deposition of oxide thin films not only introduces oxygen-doped states in the tubes, but also provides a passivation layer protecting the tubes from the external environment. Photobrightening, commonly observed in QDs and attributed to passivation of surface trap states, is also observed in these thin film coated tubes. Overall, oxide thin film coated tubes exhibit significantly higher photostability compared to that of tubes doped via ozonolysis in aqueous suspension. Hence, our method provides an easy route toward fabrication of photostable oxygen-doped SWCNTs in solid-state matrices that can be versatilely incorporated into various types of optical and optoelectronic devices that were previously hindered by single tube instabilities. Moreover, this general oxide evaporation approach to doping can be conveniently applied in the well-developed Si/SiO_2 based micro/nanodevice fabrication techniques for the development of novel devices.

4. Experimental Section

Sample Preparation: To prepare thin film coated SWCNT matrices, tubes were first chirality sorted via two-step aqueous two-phase extraction[50–52] with nonsonicated SWCNT dispersions as starting material.[53] In the subsequent cleaning process the (6,5) enriched fractions were exchanged into 1 wt% DOC, 1 wt% SDBS, or 1 wt% SDS and then stored in the dark as our final source materials for preparing the thin film coated tubes, the undoped control samples, and the tubes doped via ozonolysis. Three different types of substrates were used in this study for thin film deposition: quartz substrates, glass cover slides, and n-type Si wafers with (1 0 0) orientation. For the first two types of substrates, diluted SWCNT suspensions were directly drop-cast on the precleaned substrates, while for the Si wafer, additional layers of Au (100 nm) and SiO_2 (20–300 nm) films were deposited before drop casting the nanotube suspensions. The purpose of these two additional layers is to shield the background emission from the Si wafer in the near-infrared wavelength range. After drop casting the SWCNT suspensions, the samples were loaded into the electron beam evaporation chamber. Purities of the SiO_2 (1–3 mm pieces, CERAC, Inc.) and Al_2O_3 (1.5–4 mm pieces, Kurt J. Lesker) evaporation source materials were both 99.99%. Base pressure of the chamber was 2.8×10^{-8} Torr. Oxide thin films were deposited at the rate of 0.2 nm s^{-1} for the thin films (<10 nm) and 0.3 nm s^{-1} for the thick films (>10 nm). The substrate temperature was maintained at room temperature during the film deposition. After deposition, the samples were mounted directly into a confocal laser microscope or a continuous-flow, liquid-He cryostat for room and cryogenic temperature optical measurements, respectively.

Control samples of SWCNTs doped via ozonolysis used in this study were prepared following the method in ref. [9] with some small modifications. Briefly, chirality-sorted suspensions enriched in (6,5) SWCNTs wrapped with 1 wt% SDBS were diluted with deionized (DI) water to decrease the SDBS concentration to 0.2 wt%. Ozone saturated water was then added to the SWCNT suspensions (typically, 90 µL of ozonized water to 300 µL of SWCNT suspension), and the mixture was irradiated with a fluorescent lamp overnight (17 h). The SDBS concentration was increased back to 1 wt% after the ozonation treatments and the suspensions were stored in the dark for further measurements. To prepare samples for individual SWCNT PL measurements, typically a 5–10 µL drop of freshly diluted nanotube suspension was drop cast on precleaned substrates.

Photoluminescence Imaging and Spectroscopy Measurements: Optical PL measurements were performed on a home-built confocal laser microscope. A continuous-wave tunable Ti:Sapphire laser (Coherent) operating at 840 nm was used to excite (6,5) SWCNTs at their E_{11} phonon sideband. Infrared objectives (Olympus) with NA = 0.65, 50× magnification, and NA = 0.80, 100× magnification were used for cryogenic and room temperature measurements, respectively. PL signal from SWCNTs was collected by the objectives and spatially and spectrally imaged by a 2D InGaAs camera equipped on a 300 mm spectrograph and spectrally resolved by a linear InGaAs array equipped on a 150 mm spectrograph with typical integration time between 2 and 10 s. For wide field PL imaging, an achromatic lens was inserted to focus the incoming collimated laser beam to the back aperture of the objective. The output laser beam was quasi-homogeneous. To perform the wavelength selected wide field PL imaging, a center wavelength = 1000 nm, fwhm = 50 nm bandpass filter, and a 1045 nm long-pass filter were used for the different wavelength ranges, respectively. All cryogenic temperature experiments were performed in the temperature range between 4.2 and 5.3 K.

Supporting Information

Supporting Information is available from the Wiley Online Library or from the author.

Acknowledgments

This work was conducted at the Center for Integrated Nanotechnologies, a U.S. Department of Energy, Office of Basic Energy Sciences user facility and supported in part by Los Alamos National Laboratory (LANL) Directed Research and Development Funds. The authors thank Erik H. Haroz of LANL for insightful discussion on surfactant chemistries of SWCNTs.

Received: June 23, 2015
Revised: August 2, 2015
Published online: September 11, 2015

[1] A. Högele, C. Galland, M. Winger, A. Imamoglu, *Phys. Rev. Lett.* **2008**, *100*, 217401.
[2] J. A. Misewich, R. Martel, P. Avouris, J. C. Tsang, S. Heinze, J. Tersoff, *Science* **2003**, *300*, 783.
[3] K. Welsher, Z. Liu, S. P. Sherlock, J. T. Robinson, Z. Chen, D. Daranciang, H. Dai, *Nat. Nanotechnol.* **2009**, *4*, 773.

[4] P. W. Barone, S. Baik, D. A. Heller, M. S. Strano, *Nat. Mater.* **2005**, *4*, 86.
[5] P. Avouris, M. Freitag, *Nat. Photon.* **2008**, *2*, 341.
[6] W. Walden-Newman, I. Sarpkaya, S. Strauf, *Nano Lett.* **2012**, *12*, 1934.
[7] Y. Piao, B. Meany, L. R. Powell, N. Valley, H. Kwon, G. C. Schatz, Y. Wang, *Nat. Chem.* **2013**, *5*, 840.
[8] Y. Miyauchi, M. Iwamura, S. Mouri, T. Kawazoe, M. Ohtsu, K. Matsuda, *Nat. Photon.* **2013**, *7*, 715.
[9] S. Ghosh, S. M. Bachilo, R. A. Simonette, K. M. Beckingham, R. B. Weisman, *Science* **2010**, *330*, 1656.
[10] X. Ma, L. Adamska, H. Yamaguchi, S. E. Yalcin, S. Tretiak, S. K. Doorn, H. Htoon, *ACS Nano* **2014**, *8*, 10782.
[11] M. Iwamura, N. Akizuki, Y. Miyauchi, S. Mouri, J. Shaver, Z. Gao, L. Cognet, B. Lounis, K. Matsuda, *ACS Nano* **2014**, *8*, 11254.
[12] X. Ma, N. F. Hartmann, J. K. S. Baldwin, S. K. Doorn, H. Htoon, *Nat. Nanotechnol.* **2015**, *10*, 671.
[13] S. Khasminskaya, F. Pyatkov, B. S. Flavel, W. H. Pernice, R. Krupke, *Adv. Mater.* **2014**, *26*, 3465.
[14] T. Mueller, M. Kinoshita, M. Steiner, V. Perebeinos, A. A. Bol, D. B. Farmer, P. Avouris, *Nat. Nanotechnol.* **2010**, *5*, 27.
[15] N. Mizuochi, T. Makino, H. Kato, D. Takeuchi, M. Ogura, H. Okushi, M. Nothaft, P. Neumann, A. Gali, F. Jelezko, J. Wrachtrup, S. Yamasaki, *Nat. Photon.* **2012**, *6*, 299.
[16] J. L. O'Brien, A. Furusawa, J. Vuckovic, *Nat. Photon.* **2009**, *3*, 687.
[17] F. Vialla, Y. Chassagneux, R. Ferreira, C. Roquelet, C. Diederichs, G. Cassabois, P. Roussignol, J. S. Lauret, C. Voisin, *Phys. Rev. Lett.* **2014**, *113*, 057402.
[18] H. Htoon, M. J. O'Connell, P. J. Cox, S. K. Doorn, V. I. Klimov, *Phys. Rev. Lett.* **2004**, *93*, 027401.
[19] M. Zheng, B. A. Diner, *J. Am. Chem. Soc.* **2004**, *126*, 15490.
[20] M. J. O'Connell, E. E. Eibergen, S. K. Doorn, *Nat. Mater.* **2005**, *4*, 412.
[21] J. J. Crochet, J. G. Duque, J. H. Werner, S. K. Doorn, *Nat. Nanotechnol.* **2012**, *7*, 126.
[22] P. M. Koenraad, M. E. Flatte, *Nat. Mater.* **2011**, *10*, 91.
[23] K. L. Chopra, *Thin Film Phenomena*, McGraw-Hill, New York, NY, USA **1969**.
[24] M. Ohring, *The Materials Science of Thin Films*, Academic Press, San Diego, CA, USA **1992**.
[25] W. Wenseleers, I. I. Vlasov, E. Goovaerts, E. D. Obraztsova, A. S. Lobach, A. Bouwen, *Adv. Funct. Mater.* **2004**, *14*, 1105.
[26] J. A. Fagan, M. Zheng, V. Rastogi, J. R. Simpson, C. Y. Khripin, C. A. S. Batista, A. R. H. Walker, *ACS Nano* **2013**, *7*, 3373.
[27] R. Haggenmueller, S. S. Rahatekar, J. A. Fagan, J. Chun, M. L. Becker, R. R. Naik, T. Krauss, L. Carlson, J. F. Kadla, P. C. Trulove, D. F. Fox, H. C. DeLong, Z. Fang, S. O. Kelley, J. W. Gilman, *Langmuir* **2008**, *24*, 5070.
[28] M. F. Islam, E. Rojas, D. M. Bergey, A. T. Johnson, A. G. Yodh, *Nano Lett.* **2003**, *3*, 269.
[29] V. C. Moore, M. S. Strano, E. H. Haroz, R. H. Hauge, R. E. Smalley, *Nano Lett.* **2003**, *3*, 1379.
[30] O. Matarredona, H. Rhoads, Z. Li, J. H. Harwell, L. Balzano, D. E. Resasco, *J. Phys. Chem. B* **2003**, *107*, 13357.
[31] M. J. O'Connell, S. M. Bachilo, C. B. Huffman, V. C. Moore, M. S. Strano, E. H. Haroz, K. L. Rialon, P. J. Boul, W. H. Noon, C. Kittrell, J. Ma, R. H. Hauge, R. B. Weisman, R. E. Smalley, *Science* **2002**, *297*, 593.
[32] K. Yurekli, C. A. Mitchell, R. Krishnamoorti, *J. Am. Chem. Soc.* **2004**, *126*, 9902.
[33] T. J. McDonald, C. Engtrakul, M. Jones, G. Rumbles, M. J. Heben, *J. Phys. Chem. B* **2006**, *110*, 25339.
[34] N. R. Tummala, A. Striolo, *ACS Nano* **2009**, *3*, 595.
[35] S. Lin, D. BlankSchtein, *J. Phys. Chem. B* **2010**, *114*, 15616.
[36] M. Suttipong, N. R. Tummala, K. B, A. Striolo, *J. Phys. Chem. C* **2011**, *115*, 17286.
[37] J. G. Duque, C. G. Densmore, S. K. Doorn, *J. Am. Chem. Soc.* **2010**, *132*, 16165.
[38] M. Jose-Yacaman, M. Miki-Yoshida, L. Rendon, J. G. Santiesteban, *Appl. Phys. Lett.* **1993**, *62*, 657.
[39] J. H. Hafner, M. J. Bronikowski, B. R. Azamian, P. Nikolaev, A. G. Rinzler, D. T. Colbert, K. A. Smith, R. E. Smalley, *Chem. Phys. Lett.* **1998**, *296*, 195.
[40] A. M. Cassell, J. A. Raymakers, J. Kong, H. Dai, *J. Phys. Chem. B* **1999**, *103*, 6484.
[41] J. G. Duque, C. E. Hamilton, G. Gupta, S. A. Crooker, J. J. Crochet, A. Mohite, H. Htoon, K. A. D. Obrey, A. M. Dattelbaum, S. K. Doorn, *ACS Nano* **2011**, *8*, 6686.
[42] M. Kuno, D. P. Fromm, H. F. Hamann, A. Gallagher, D. J. Nesbitt, *J. Chem. Phys.* **2000**, *112*, 3117.
[43] M. Jones, J. Nedeljkovic, R. J. Ellingson, A. J. Nozik, G. Rumbles, *J. Phys. Chem. B* **2003**, *107*, 11346.
[44] J. Kimura, T. Uematsu, S. Maenosono, Y. Yamaguchi, *J. Phys. Chem. B* **2004**, *108*, 13258.
[45] D. B. Tice, M. T. Frederick, R. P. H. Chang, E. A. Weiss, *J. Phys. Chem. C* **2011**, *115*, 3654.
[46] J. J. Peterson, T. D. Krauss, *Phys. Chem. Chem. Phys.* **2006**, *8*, 3851.
[47] A. L. Weaver, D. R. Gamelin, *J. Am. Chem. Soc.* **2012**, *134*, 6819.
[48] S. Sarkar, A. K. Guria, B. K. Patra, N. Pradhan, *Nanoscale* **2014**, *6*, 3786.
[49] M. Oda, M. Y. Shen, M. Saito, T. Goto, *J. Lumin.* **2000**, *87*, 469.
[50] C. Y. Khripin, J. A. Fagan, M. Zheng, *J. Am. Chem. Soc.* **2013**, *135*, 6822.
[51] J. A. Fagan, C. Y. Khripin, C. A. Silvera Batista, J. R. Simpson, E. H. Hároz, A. R. Hight Walker, M. Zheng, *Adv. Mater.* **2014**, *26*, 2800.
[52] N. K. Subbaiyan, S. Cambré, A. N. G. Parra-Vasquez, E. H. Hároz, S. K. Doorn, J. G. Duque, *ACS Nano* **2014**, *8*, 1619.
[53] N. K. Subbaiyan, A. N. G. Parra-Vasquez, S. Cambré, M. A. Santiago Cordoba, S. E. Yalcin, E. C. Hamilton, N. H. Mack, J. L. Blackburn, S. K. Doorn, J. G. Duque, *Nano Research* **2015**, *9*, 4043.